

# LoGG3D-Net: Locally Guided Global Descriptor Learning for 3D Place Recognition

Kavisha Vidanapathirana<sup>1,2</sup>, Milad Ramezani<sup>1</sup>, Peyman Moghadam<sup>1,2</sup>,  
Sridha Sridharan<sup>2</sup>, Clinton Fookes<sup>2</sup>

**Abstract**—Retrieval-based place recognition is an efficient and effective solution for enabling re-localization within a pre-built map or global data association for Simultaneous Localization and Mapping (SLAM). The accuracy of such an approach is heavily dependant on the quality of the extracted scene-level representation. While end-to-end solutions, which learn a global descriptor from input point clouds, have demonstrated promising results, such approaches are limited in their ability to enforce desirable properties at the local feature level. In this paper, we demonstrate that the inclusion of an additional training signal (local consistency loss) can guide the network to learning local features which are consistent across revisits, hence leading to more repeatable global descriptors resulting in an overall improvement in place recognition performance. We formulate our approach in an end-to-end trainable architecture called *LoGG3D-Net*. Experiments on two large-scale public benchmarks (KITTI and MulRan) show that our method achieves mean  $F1_{max}$  scores of 0.939 and 0.968 on KITTI and MulRan, respectively while operating in near real-time.

## I. INTRODUCTION

Despite considerable progress in the field of 3D point cloud perception for robotics and self-driving cars, existing methods for data-association remain fragile and limited in applicability, especially in large-scale outdoor scenes. Accurate data-association is vital for enabling long-term autonomy, as autonomous agents need to construct and maintain an accurate representation of the environment they operate in. Recognizing previously visited places provides global constraints to restrict cumulative errors within Simultaneous Localization and Mapping (SLAM) systems [1], [2]. This is known as the Place Recognition (PR) task.

Compared to visual place recognition [3], the use of 3D point clouds extracted from LiDAR sensors benefits from its inherent invariance to view-point and illumination. However extracting useful information from the point cloud representation remains a challenge due to higher sparsity and a complex and variable distribution of points. In this paper, we consider the task of place recognition on 3D point clouds.

While there have been many handcrafted approaches to extracting useful information for the task of place recognition [4]–[6], discriminative learning-based approaches have

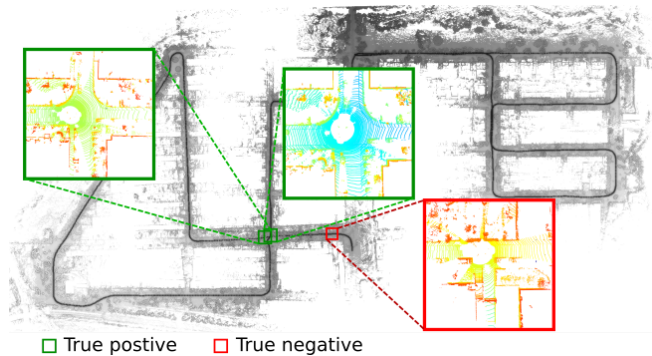


Fig. 1: Point cloud based place recognition in large-scale environments using *LoGG3D-Net*.

demonstrated competitive performance in terms of both accuracy and efficiency [7], [8].

We propose *LoGG3D-Net*, a novel end-to-end 3D place recognition method for LiDAR point clouds. Fig. 1 shows an example of retrieval results on KITTI sequence 08 which demonstrates some challenging orthogonal revisits. In contrast to state-of-the-art end-to-end methods, which rely solely on global descriptor learning, we propose to jointly optimize local and scene-level embeddings. We achieve this by introducing a local consistency loss that takes a pair of LiDAR point clouds and maximizes the similarity of their corresponding points' features and minimizes the similarity of all non-corresponding points' features.

We further introduce the use of second-order pooling followed by Eigen-value power normalization to aggregate local features and generate a global descriptor in the end-to-end setting. We note that all current learning-based methods use NetVLAD [9] or other first-order aggregation methods [10] to compute the global descriptor, and higher-order aggregation methods have not been explored in the end-to-end setting for LiDAR-based place recognition. We evaluate the accuracy and robustness of *LoGG3D-Net* on 6 KITTI sequences and 5 sequences of the MulRan dataset. Note that these datasets are collected using different LiDAR sensors (Velodyne HDL-64E in KITTI, Ouster OS1-64 in MulRan) and different countries (Germany, Korea). Our main contributions are summarized as follows:

- We introduce an additional training signal that can be used in the end-to-end global descriptor learning setting that allows to enforce consistency of the local embeddings extracted from point clouds of the same location.

<sup>1</sup> Kavisha Vidanapathirana, Milad Ramezani and Peyman Moghadam are with the Robotics and Autonomous Systems Group, DATA61, CSIRO, Brisbane, QLD 4069, Australia. E-mails: *firstname.lastname@data61.csiro.au*

<sup>2</sup> Kavisha Vidanapathirana, Peyman Moghadam, Sridha Sridharan, Clinton Fookes are with the School of Electrical Engineering and Robotics, Queensland University of Technology (QUT), Brisbane, Australia. E-mails: {*kavisha.vidanapathirana, peyman.moghadam, s.sridharan, c.fookes*}@qut.edu.au

We demonstrate how including this property in the local features contributes towards better performance of the global descriptor.

- We introduce the use of second-order pooling in the end-to-end setting for LiDAR-based place recognition as we believe it has more representative power compared to the commonly used first-order aggregation methods.
- Using 2 large scale public datasets, we demonstrate the superiority of our method in the end-to-end setting while operating in near real-time.

The remainder of this paper is organized as follows. In Sec. II we discuss related work. Sec. III explains our proposed method. The experimental setup is outlined in Sec. IV. Sec. V discusses the experimental results and concluding remarks are provided in Sec. VI.

## II. RELATED WORK

Solutions for 3D LiDAR-based place recognition can be loosely classified under retrieval-based methods and local-feature matching based methods. Local feature matching based methods rely on accurate pose estimates to limit the search space of feature correspondences and hence do not scale well for the task of re-localization in large-scale environments. Majority of local feature matching based approaches operate by detecting keypoints and describing their local neighborhood [6], [11]. Recently features extracted from larger local regions such as point segments have shown superior performance [12], [13].

Retrieval-based methods are inexpensive due to simple matching of global descriptors and therefore scale well to large-scale scenarios. Retrieval-based methods operate by encoding each point cloud to a single compact vector representation that can be used for querying a database of previously visited places. Global descriptors can be categorized as handcrafted [4], [5], hybrid [14], and end-to-end learning-based [7]. Handcrafted methods have the benefit of not needing retraining to adapt to different environments and sensor-types. Prominent methods such as ScanContext [5] have demonstrated reliable performance in various scenarios. However the discriminative power of such methods remains limited.

End-to-end methods formulate the learning of global descriptors using a contrastive approach to obtain discriminative scene representations. PointNetVLAD [7] pioneered the use of an end-to-end trainable global descriptor for 3D point cloud place recognition. PointNetVLAD extracts local features from PointNet [15] and employs the NetVLAD aggregator [9] to form a global descriptor of the scene. To address the limited descriptive power of the PointNet backbone, other approaches such as LPD-Net [16] have been proposed. More recently MinkLoc3D [8] proposed an efficient architecture outperforming its end-to-end predecessors. MinkLoc3D utilized sparse convolutions which have been demonstrated to be effective at capturing useful point-level features. We also benefit from the use of sparse convolutions.

We note that all end-to-end methods rely solely on supervisory signals applied on the global descriptors. Additionally, all end-to-end methods are currently utilizing first-order aggregation methods in the formulation of the global descriptors. In many visual recognition tasks, higher-order aggregation methods have demonstrated superior performance [17]–[19]. In this work, we address the above limitations by introducing an additional training signal to the local features, and using second-order pooling for global descriptor generation respectively.

## III. PROPOSED METHOD

The overall architecture of our *LoGG3D-Net* is presented in Fig. 2. Given a raw point cloud input, a sparse convolution-based U-Net (SparseConv U-Net) is used to embed each point into a high dimensional feature space. Then, it uses a pair of LiDAR point clouds from a nearby location with considerable overlap of points and a ‘Local Consistency Loss’ to maximise the similarity of corresponding points’ features in the embedding space. Next, local features are aggregated using a second-order pooling followed by a Eigen-value power normalisation to form a global scene-level descriptor. A quadruplet loss is used to train our scene-level global descriptors. Finally, we combine our local consistency loss with our scene-level loss to optimize our network.

### A. Problem Formulation

The task of point cloud-based retrieval for place recognition is generally formulated as follows. Given a point cloud  $\mathcal{P} \in \mathbb{R}^{N \times 4}$  representing varying number of  $N$  points with associated  $x, y, z$  and intensity, a mapping function  $\Phi : \mathcal{P} \rightarrow g \in \mathbb{R}^{d'}$  is developed that represents the point cloud with a fixed-size global descriptor  $g$ . End-to-end learning of global descriptors is formulated as follows:

**Problem:** Given a training set  $\{\mathcal{S}_i\} = \{(\mathcal{P}_i, \mathbf{x}_i)\}$  consisting of pairs of point cloud  $\mathcal{P}_i$  with associated geo-location  $\mathbf{x}_i$ , find the parameters  $\theta$  of the mapping function  $\Phi_\theta : \mathcal{P} \rightarrow g \in \mathbb{R}^{d'}$ , such that for any subset of samples  $\{\mathcal{S}_a, \mathcal{S}_i, \mathcal{S}_j\}$ ,

$$\mathcal{D}(\mathbf{x}_a, \mathbf{x}_i) \leq \mathcal{D}(\mathbf{x}_a, \mathbf{x}_j) \implies \|g_a - g_i\| \leq \|g_a - g_j\|, \quad (1)$$

where,  $\mathcal{D}$  represents geometric distance and  $\|\cdot\|$  represents a distance in the feature space (typically  $L_2$ ).

Learning the parameter  $\theta$  that addresses the above problem is generally performed using a metric learning setting by applying a loss function  $\mathcal{L}_g$  that acts on the global descriptors extracted from a tuple  $\mathcal{T}$  of training samples. We use the subscript ‘ $g$ ’ in  $\mathcal{L}_g$  to highlight that the loss is typically only applied on the global descriptors, *i.e.*, at the scene-level.

### B. Our Approach

We note that generally  $\Phi$  can be decomposed into two functions such that,

$$\Phi \equiv \varphi \circ \phi, \quad (2)$$

where,  $\phi : \mathcal{P} \rightarrow \{f\}$  extracts local features  $f \in \mathbb{R}^d$ , and  $\varphi : \{f\} \rightarrow g$  aggregates the local features into a single global descriptor  $g$ . Under this setting, optimizing  $\theta$  with

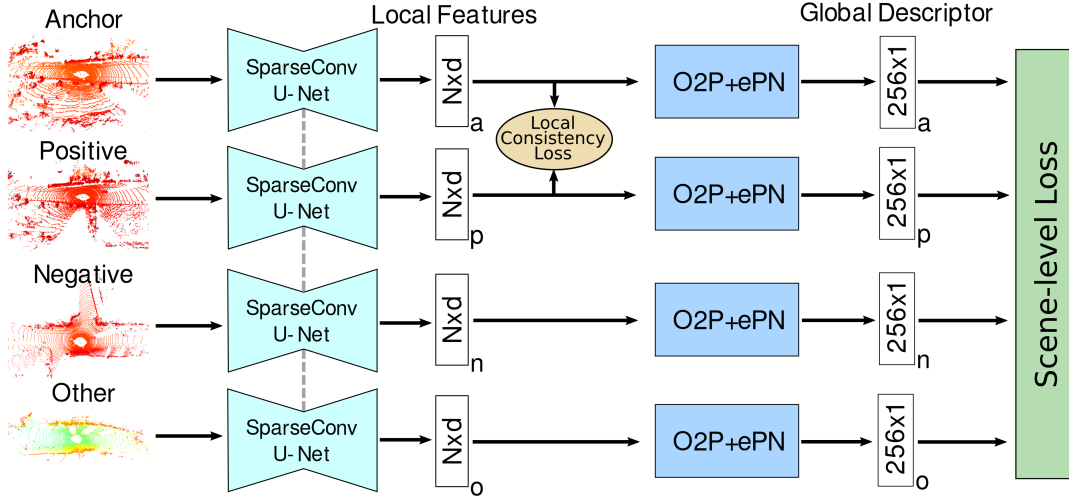


Fig. 2: An overview of the proposed *LoGG3D-Net* method. A quadruplet of point clouds are fed into a SparseConv U-Net. The local consistency loss is applied to the anchor and positive point clouds to explicitly enforce consistency of local feature embeddings. The local features are aggregated using second-order pooling (O2P) followed by a Eigen-value Power Normalization (ePN) to obtain a global descriptor. The final loss is the combination of the local consistency loss with the scene-level loss.

a training signal applied only to the global descriptor seems limited, *i.e.*, there are desirable properties of the intermediate representations  $\{f\}$  (local features) that cannot be fully enforced by  $\mathcal{L}_g$ .

**Hypothesis:** Given two point clouds from the nearby location (*i.e.*, with considerable overlap of points), enforcing consistency of local features of corresponding points will result in a more repeatable global descriptors after aggregation.

We define ‘corresponding points’ are two points from different point clouds that are nearby when represented with respect to a global coordinate frame. ‘Consistency of local features’ implies that local features of corresponding points should be nearby in the embedding space. Towards testing the above hypothesis, we introduce an additional training signal to enforce features  $\{f\}$  of corresponding points to be consistent in the embedding space.

### C. Local Descriptor

For the local feature extractor  $\phi$ , we use a Sparse U-Net style backbone [20] which performs sparse point-voxel convolution. The backbone consists of two branches: the voxel-based branch and point-based branch. The voxel-based branch learns local neighborhood information at varying receptive field sizes, and the point-based branch learns high-resolution information that may be lost in the voxelized branch. The information across the two branches are fused at intermediate steps to capture complementary information from the input 3D point clouds.

1) *Point Correspondences:* Given a pair of samples  $\{S_1, S_2\}$  from the nearby location (*i.e.*  $d(x_1, x_2) < \tau$ ), the corresponding points in the two point clouds  $\{P_1, P_2\}$  are calculated by first transforming the point clouds to a common coordinate frame using the geo-location information  $\{x_1, x_2\}$  followed by ICP [21] for better alignment (to account for

possible errors in geo-locations). After alignment, point correspondences can be found using radius-based nearest neighbor search between the two point clouds. This search is made efficient using approximate nearest neighbor search algorithm FLANN [22]. For each point  $^1p_i$  in point cloud  $P_1$  and radius  $r$ , the corresponding points in point cloud  $P_2$  are found as  $C_i^{12} = \{(i, j) \mid \mathcal{D}(^1p_i, ^2p_j) < r\}$ . The set of corresponding points between the two point clouds is represented as  $C^{12}$ .

2) *Local Consistency Loss:* Given two samples  $\{S_1, S_2\}$ , the associated local features  $\{\{f\}_1, \{f\}_2\}$  and the point correspondences  $C^{12}$ , a contrastive loss is applied to minimize the distance for features of corresponding points (positive pairs) while maximizing the distance of features of non-corresponding points (negative pairs). We adopt the Hardest-Contrastive loss in FCGF [23] which is defined as,

$$\begin{aligned} \mathcal{L}_{lc} = & \sum_{(i,j) \in C^{12}} \left\{ \left[ \|f(^1p_i) - f(^2p_j)\|_2^2 - m_p \right]_+ / |C^{12}| \right. \\ & + \lambda_n I_i \left[ m_n - \min_{k \in \mathcal{M}} \|f(^1p_i) - f(^2p_k)\|_2^2 \right]_+ / |C_1^{12}| \\ & \left. + \lambda_n I_j \left[ m_n - \min_{k \in \mathcal{M}} \|f(^2p_j) - f(^1p_k)\|_2^2 \right]_+ / |C_2^{12}| \right\}, \end{aligned} \quad (3)$$

where,  $\mathcal{M}$  is a subset of random non-corresponding features used for hard negative mining and  $[\cdot]_+$  denotes the hinge loss.  $I_i$  is short for  $I(i, k_i, r)$ , which is an indicator function that returns 1 if the point  $k_i$  is non-corresponding (outside radius  $r$ ) to point  $i$  and 0 otherwise, where  $k_i = \text{argmin}_{k \in \mathcal{M}} \mathcal{D}(f_i, f_k)$ .  $|C_1^{12}| = \sum_{(i,j) \in C^{12}} I(i, k_i, r)$  is the number of valid mined negatives for the first item ( $|C_2^{12}|$  for the second item) throughout the point cloud.  $\lambda_n$  is set to 0.5

in our method.

The local consistency loss  $\mathcal{L}_{lc}$  acts on the parameters of  $\phi$  in the decomposition of Eq. (2) to get well-formed repeatable local features.

#### D. Global Descriptor

Given a point cloud  $\mathcal{P} = \{p_i\}$  and the set of point features  $\{f(p_i)\}$  where  $f(p_i) \in \mathbb{R}^d$ , the second-order pooling  $F^{O_2}$  of the features is defined as,

$$F^{O_2} = \{F_{xy}^{O_2}\}, \quad F_{xy}^{O_2} = \max_{p_i \in \mathcal{P}} f_{xy}^{o_2}(p_i), \quad (4)$$

where  $F^{O_2}$  is a matrix with elements  $F_{xy}^{O_2} (1 \leq x, y \leq d)$  and  $f^{o_2}(p_i) = f(p_i)f(p_i)^T \in \mathbb{R}^{d \times d}$  is the outer product of the point feature with itself. This accounts to taking the element-wise maximum of the second-order features of all points in the point cloud.

In order to make the scene descriptor matrix  $F^{O_2}$  more discriminative, we use Eigen-value Power Normalization (ePN) [17]–[19]. Given the singular value decomposition  $F^{O_2} = U\lambda V^T$  the ePN result  $F_\alpha^{O_2}$  is obtained by raising each of the singular values by a power of  $\alpha$  as follows,

$$F_\alpha^{O_2} = U\hat{\lambda}V^T, \quad \hat{\lambda} = \text{diag}(\lambda_{1,1}^\alpha, \dots, \lambda_{d,d}^\alpha), \quad (5)$$

where,  $\alpha = 0.5$ . The matrix  $F_\alpha^{O_2}$  is flattened and normalized to obtain the final global descriptor vector  $g \in \mathbb{R}^{d^2}$ .

After the aggregation of point features into a global descriptor using second-order pooling, the scene-level loss  $\mathcal{L}_g$  is applied to a tuple  $\mathcal{T}$  of training samples. We use the quadruplet loss [24] where a tuple is denoted as  $\mathcal{T}_i = (\mathcal{S}_a, \{\mathcal{S}_p\}, \{\mathcal{S}_n\}, \mathcal{S}_{n^*})$ , where  $\mathcal{S}_a$  is the anchor sample,  $\{\mathcal{S}_p\}$  a set of positives (such that  $d(\mathbf{x}_a, \mathbf{x}_p) < \tau_p$ ),  $\{\mathcal{S}_n\}$  a set of negatives (such that  $d(\mathbf{x}_a, \mathbf{x}_n) > \tau_n$ ), and  $\mathcal{S}_{n^*}$  is sampled such that it is not a positive to the query nor to all previous negatives (such that  $d(\mathbf{x}_{n^*}, \mathbf{x}) > \tau_p \forall \mathbf{x} = \{\mathbf{x}_a, \mathbf{x}_n\}$ ).

In each tuple we first find the hardest positive sample,

$$\mathcal{P}_{hp} = \max_{\mathcal{P}_{p^i} \in \{\mathcal{P}_p\}} \|g(\mathcal{P}_a) - g(\mathcal{P}_{p^i})\|_2, \quad (6)$$

The quadruplet loss is then defined as:

$$\mathcal{L}_g = \sum_i^{\mathcal{N}} \left\{ \left[ \|g(\mathcal{P}_a) - g(\mathcal{P}_{hp})\|_2^2 - \|g(\mathcal{P}_a) - g(\mathcal{P}_{n^i})\|_2^2 + \alpha \right]_+ + \left[ \|g(\mathcal{P}_a) - g(\mathcal{P}_{hp})\|_2^2 - \|g(\mathcal{P}_{n^*}) - g(\mathcal{P}_{n^i})\|_2^2 + \beta \right]_+ \right\}, \quad (7)$$

where,  $\alpha$  and  $\beta$  are constant margins and  $\mathcal{N}$  is the number of sampled negatives.

#### E. Joint Local and Global Loss

Our network is jointly optimized by a weighted sum of the global scene-level loss and the local consistency loss described as:

$$\mathcal{L} = \mathcal{L}_g + \omega \cdot \mathcal{L}_{lc} \quad (8)$$

where,  $\omega$  is a scalar hyperparameter term.

## IV. EXPERIMENTAL SETUP

### A. Implementation and Training Setup

The proposed network is implemented using the PyTorch framework and trained on 12 Nvidia Tesla P100-16GB GPUs using DistributedDataParallel. The TorchSparse library [20] is used for sparse convolutions. During training, the ground plane is first removed using RANSAC plane fitting followed by down-sampling using a voxel grid filter of 10cm. Finally, input point clouds are limited to a maximum of 35K points. To reduce overfitting, we apply the following data augmentations for training. Random point jitter is introduced using Gaussian noise sampled from  $\mathcal{N}(\mu = 0, \sigma = 0.01)$  clipped at 0.03m. Each point cloud is also randomly rotated about the  $z$ -axis by an angle between  $\pm 180^\circ$ . Note that ground plane removal is not used during evaluation to speed up inference time as it does not affect evaluation performance of our proposed method.

The dimensionality of the local features is set to 16 which results in a 256 dimension global descriptor for fair comparison with PointNetVLAD. In the local consistency loss  $\mathcal{L}_{lc}$ , the margins  $m_p$  and  $m_n$  are set to 0.1 and 2.0, respectively. The local consistency loss is only applied to randomly sampled 5192 positive pairs similar to FCGF [23]. The quadruplet loss margins are set to  $\alpha = 0.5$  and  $\beta = 0.3$ . The distances for sampling positive and negative point cloud pairs are set to  $\tau_p = 3m$  and  $\tau_n = 20m$ . For  $\mathcal{L}_g$  we use 2 positives, 9 negatives and 1 other negative. We train our model using Adam optimizer with an initial learning rate of 0.001 and a multi-step scheduler to drop the learning rate by a factor of 10 after 10 epochs and train until convergence for a maximum of 24 hours.

### B. Datasets

We evaluate the proposed method on two public LiDAR datasets (KITTI, MulRan), both of which were collected from a moving vehicle in multiple dynamic urban environments. Note that these datasets are collected using different LiDAR sensors (Velodyne HDL-64E in KITTI, Ouster OS1-64 in MulRan) and different countries (Germany, Korea).

**KITTI:** The KITTI odometry dataset [25] contains 11 sequences of Velodyne HDL-64E LiDAR scans collected in Karlsruhe, Germany. We train on these 11 sequences using the leave-one-out cross-validation strategy and evaluate on the 6 sequences with revisits (00, 02, 05, 06, 07 and 08).

**MulRan:** The MulRan dataset [26] contains scans collected from an Ouster-64 sensor from multiple environments in South Korea. The dataset contains 12 sequences, 9 of which we use for evaluation. We train on DCC1, DCC2, Riverside1 and Riverside3 sequences and evaluate on the remaining sequences of DCC, Riverside and KAIST. To evaluate the generalization capabilities of methods, the KAIST sequences are unseen test sets for evaluation.

### C. Evaluation Criteria

We compute the similarity between the global descriptors of each query point cloud with a database of global

Method	DCC2	Riverside2	mean
$\mathcal{L}_g$	0.355	0.472	0.413
$\mathcal{L}_g + 0.1 \cdot \mathcal{L}_{lc}$	0.471	0.578	0.524
$\mathcal{L}_g + 1.0 \cdot \mathcal{L}_{lc}$	<b>0.591</b>	<b>0.747</b>	<b>0.669</b>

TABLE I: Ablation study of the effects of  $\omega$  term for our joint loss.  $\mathcal{L}_g$  is the scene-level loss and  $\mathcal{L}_{lc}$  is the local consistency loss.

descriptors of previously seen point clouds in each sequence. Previous entries adjacent to the query by less than  $t_r$  time difference are excluded from the search to avoid matching to the same instance. For  $t_r$  we use 30s and 90s for KITTI and MulRan, respectively. Methods are compared using the Precision-Recall curve and its scalar metric the maximum  $F1$  score ( $F1_{max}$ ).

## V. RESULTS

In this section we first demonstrate the performance improvement from the inclusion of  $\mathcal{L}_{lc}$ . We evaluate our method in comparison to other state-of-the-art methods and conduct a run-time analysis to judge the suitability of methods for real-time operation.

### A. Ablation study on point-wise loss

We evaluate the effect of inclusion of the local consistency loss through an ablation study on selected sequences of the MulRan dataset. We train on sequences DCC1, Riverside1 and evaluate performance on DCC2 and Riverside2. Table I summarizes the  $F1_{max}$  for each test sequence by varying the weight of the local consistency loss  $\omega$  in Eq. (8). It is evident that the inclusion on the local consistency loss leads to an improvement in place recognition performance.  $\omega = 0.1$  leads to an improvement of 26% mean  $F1_{max}$  with respect to the baseline while  $\omega = 1.0$  leads to an improvement of 61% leading to the best performance. All the following experiments are carried out with  $\omega = 1.0$ .

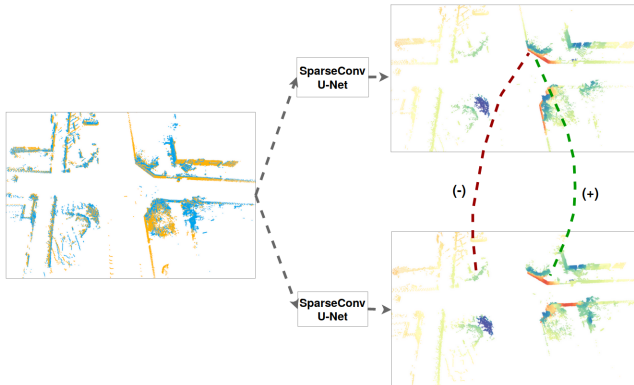
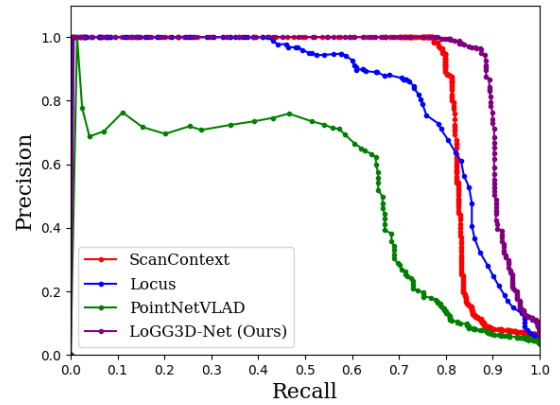
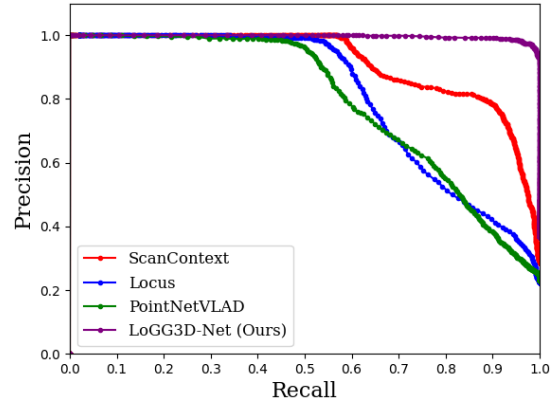


Fig. 3: t-SNE of point-features extracted from two point clouds of the same location shows that our method produces ‘locally consistent’ features. This property leads to more repeatable global descriptors after aggregation. Colors represent the similarity of local features associated to the points of one cloud relative to one another.



(a) KITTI 02.



(b) MulRan DCC 03.

Fig. 4: Precision-Recall curves for evaluation on select sequences of the KITTI and MulRan datasets.

A qualitative depiction of the effect of  $\mathcal{L}_{lc}$  is shown in Fig. 3 between two point clouds extracted from the nearby location. The left half shows the alignment of the point cloud after ground plane removal to estimate point correspondences during training. The right half shows the two point clouds separately with each point colored based on the t-SNE embedding of the local features extracted using our pre-trained model (note that point correspondence information is not used during inference). The visualization clearly highlights that distinct regions in a single point cloud are in distinct regions in the feature space. Additionally, across point clouds, similar regions have corresponding point features implying that the local features extracted from our method are repeatable.

### B. Comparison to State-of-the-Art

We compare *LoGG3D-Net* with the state-of-the-art hand-crafted method *ScanContext*<sup>1</sup> [5], recently proposed hybrid method *Locus*<sup>2</sup> [14], and the popular end-to-end method *PointNetVLAD* [7]. For *ScanContext* we use the python version of the code provided by the authors. We use the 20x60 descriptor size and use ring-key search to find the top-10 candidates for descriptor matching. For *PointNetVLAD*

<sup>1</sup><https://github.com/irapkaist/scancontext>

<sup>2</sup><https://github.com/csiro-robotics/locus>

	KITTI							MulRan					
	00	02	05	06	07	08	mean	K1	K2	K3	D3	R2	mean
ScanContext [5]	0.966	0.871	0.914	0.985	0.698	0.610	0.841	0.954	<b>0.969</b>	<b>0.994</b>	0.893	0.826	0.916
PointNetVLAD [7]	0.909	0.637	0.859	0.924	0.171	0.437	0.656	0.952	0.856	0.979	0.685	0.868	0.868
Locus [14]	<b>0.983</b>	0.762	<b>0.981</b>	<b>0.992</b>	<b>1.000</b>	<b>0.931</b>	<b>0.942</b>	0.938	0.874	0.969	0.718	<b>0.994</b>	0.899
<b>LoGG3D-Net (Ours)</b>	0.953	<b>0.888</b>	0.976	0.977	<b>1.000</b>	0.843	0.939	<b>0.966</b>	0.938	0.991	<b>0.977</b>	0.969	<b>0.968</b>

TABLE II: Evaluation of sequential place recognition on KITTI and MulRan datasets using  $F1_{max}$  metric under the  $3m, 20m$  revisit criteria. The rows are grouped as handcrafted, hybrid, and end-to-end learning-based respectively.

we use a PyTorch-based re-implementation of the original tensorflow implementation<sup>3</sup>.

The results are summarized in Table II. On the KITTI dataset, Locus remains the highest performing method with a mean  $F1_{max}$  score 1% higher than ours. On the MulRan dataset we obtain the best mean  $F1_{max}$  score which is 5% higher than the next best performing method, *i.e.*, ScanContext. It should be noted that the local feature extractor of Locus was trained on the KITTI sequences 05 and 06 thus leading to its extremely high performance on KITTI and relatively low performance on MulRan.

Precision-Recall plots for the sequences KITTI 02 and DCC 03 are depicted in Fig. 4. KITTI 02 contains several repetitive environments and a single revisit to an intersection in the opposite direction. DCC 03 contains long traversals of revisits from the reverse direction. All these scenarios prove challenging for most methods while the adverse effect on the performance of *LoGG3D-Net* is not as pronounced.

It is worth noting that the feature dimensions of Locus and ScanContext give these methods an unfair advantage in terms of representation power. The ScanContext descriptor is  $20 \times 60$  which is a total of 1200 floating point numbers and the Locus descriptor is 4096 dimensions. Both *LoGG3D-Net* and PointNetVLAD have descriptor sizes of 256 which are compact and scale well to large databases essential for real-time robotics applications.

### C. Runtime Analysis

We tabulated the computation time for pre-processing, description and querying in Table III. Since the time for retrieval increases with the size of the database, we present the average retrieval time for all methods on MulRan DCC1 which consists of 5541 point clouds. ScanContext uses ring-key retrieval to find the top-10 candidates for full descriptor distance calculation.

The results show that Locus has very high pre-processing time due to ground-plane removal and a high description time (due to around 30-80 sequential forward passes through the segment feature extraction network which is not parallelized and hence takes  $550ms$  on average per point cloud). ScanContext has very high retrieval time even after limiting the number of ring-key candidates to just 10. The need for cosine similarity computation on each column shifted variant of the descriptor increases the descriptors query time. PointNetVLAD is the most efficient method for descriptor extraction due to its light network architecture. However,

we note that PointNetVLAD uses a considerable amount of pre-processing to first remove the ground plane and then iteratively downsample the point cloud to exactly 4096 points which makes its total time longer than ours.

Our method has acceptable description and retrieval time allowing it to run at near real-time ( $\sim 7Hz$ ). This enables its integration into SLAM systems as loop closure detection module.

	Pre-proc.	Description	Querying	Total
ScanContext [5]	63	582	3968	4613
PointNetVLAD [7]	534	7	34	575
Locus [14]	573	633	113	1319
<b>LoGG3D-Net (Ours)</b>	25	66	38	<b>139</b>

TABLE III: Runtime analysis: Average time taken on MulRan DCC1 (in ms).

## VI. CONCLUSION

This paper presented an end-to-end deep learning-based place recognition approach for LiDAR point clouds, named *LoGG3D-Net*. The model is based on a SparseConv U-Net backbone to embed local features. We introduced a local consistency loss to preserve the similarity between local feature embeddings of two overlapping point clouds (anchor and positive). Our global descriptor also ensures that point clouds are encoded into a single viewpoint invariant representation using second-order pooling, which better captures the distribution of features. We evaluated *LoGG3D-Net* on 11 sequences of two large-scale public benchmarks (KITTI and MulRan) and achieve mean  $F1_{max}$  scores of 0.939 and 0.968 on KITTI and MulRan, respectively. Ablation studies performed demonstrate that the local consistency loss provides a consistent and significant improvement, with *LoGG3D-Net* outperforming state-of-the-art place recognition methods on KITTI and MulRan datasets. Future work will consider the addition of an attention mechanism to the backbone to better exploit the most relevant information within the point clouds.

## REFERENCES

- [1] C. Park, P. Moghadam, S. Kim, A. Elfes, C. Fookes, and S. Sridharan, "Elastic LiDAR Fusion: Dense Map-Centric Continuous-Time SLAM," in *Proceedings - IEEE International Conference on Robotics and Automation*, sep 2018, pp. 1206–1213.
- [2] C. Park, P. Moghadam, J. L. Williams, S. Kim, S. Sridharan, and C. Fookes, "Elasticity Meets Continuous-Time: Map-Centric Dense 3D LiDAR SLAM," *IEEE Transactions on Robotics*, 2021.
- [3] S. Lowry, N. Sunderhauf, P. Newman, J. J. Leonard, D. Cox, P. Corke, and M. J. Milford, "Visual Place Recognition: A Survey," *IEEE Transactions on Robotics*, vol. 32, no. 1, pp. 1–19, feb 2016.

<sup>3</sup><https://github.com/mikacuy/pointnetvlad>



- [4] L. He, X. Wang, and H. Zhang, "M2DP: A Novel 3D Point Cloud Descriptor and Its Application in Loop Closure Detection," in *IEEE International Conference on Intelligent Robots and Systems*, nov 2016, pp. 231–237.
- [5] G. Kim and A. Kim, "Scan Context: Egocentric Spatial Descriptor for Place Recognition Within 3D Point Cloud Map," in *IEEE International Conference on Intelligent Robots and Systems*, dec 2018, pp. 4802–4809.
- [6] S. Salti, F. Tombari, and L. Di Stefano, "SHOT: Unique signatures of histograms for surface and texture description," *Computer Vision and Image Understanding*, vol. 125, pp. 251–264, 2014.
- [7] M. A. Uy and G. H. Lee, "PointNetVLAD: Deep Point Cloud Based Retrieval for Large-Scale Place Recognition," in *Proceedings of the IEEE Computer Society Conference on Computer Vision and Pattern Recognition*, dec 2018, pp. 4470–4479.
- [8] J. Komorowski, "MinkLoc3D: Point Cloud Based Large-Scale Place Recognition," in *Proceedings of the IEEE/CVF Winter Conference on Applications of Computer Vision (WACV)*, January 2021, pp. 1790–1799.
- [9] R. Arandjelovic, P. Gronat, A. Torii, T. Pajdla, and J. Sivic, "NetVLAD: CNN architecture for weakly supervised place recognition," in *Proceedings of the IEEE Computer Society Conference on Computer Vision and Pattern Recognition*, vol. 2016-Decem. IEEE Computer Society, dec 2016, pp. 5297–5307.
- [10] F. Radenović, G. Tolias, and O. Chum, "Fine-tuning cnn image retrieval with no human annotation," *IEEE Transactions on Pattern Analysis and Machine Intelligence*, vol. 41, no. 7, pp. 1655–1668, 2019.
- [11] J. Guo, P. V. Borges, C. Park, and A. Gawel, "Local Descriptor for Robust Place Recognition Using LiDAR Intensity," *IEEE Robotics and Automation Letters*, vol. 4, no. 2, pp. 1470–1477, apr 2019.
- [12] R. Dubé, A. Cramariuc, D. Dugas, H. Sommer, M. Dymczyk, J. Nieto, R. Siegwart, and C. Cadena, "Segmap: Segment-based mapping and localization using data-driven descriptors," *The International Journal of Robotics Research*, vol. 39, no. 2-3, pp. 339–355, 2020. [Online]. Available: <https://doi.org/10.1177/0278364919863090>
- [13] G. Tinchev, A. Penate-Sanchez, and M. Fallon, "Learning to See the Wood for the Trees: Deep Laser Localization in Urban and Natural Environments on a CPU," *IEEE Robotics and Automation Letters*, vol. 4, no. 2, pp. 1327–1334, 2019.
- [14] K. Vidanapathirana, P. Moghadam, B. Harwood, M. Zhao, S. Sridharan, and C. Fookes, "Locus: LiDAR-based Place Recognition using Spatiotemporal Higher-Order Pooling," in *2021 IEEE International Conference on Robotics and Automation (ICRA)*, 2021.
- [15] C. R. Qi, H. Su, K. Mo, and L. J. Guibas, "PointNet: Deep Learning on Point Sets for 3D Classification and Segmentation," in *Proceedings of the IEEE Conference on Computer Vision and Pattern Recognition (CVPR)*, July 2017.
- [16] Z. Liu, S. Zhou, C. Suo, P. Yin, W. Chen, H. Wang, H. Li, and Y. Liu, "LPD-Net: 3D Point Cloud Learning for Large-Scale Place Recognition and Environment Analysis," in *2019 IEEE/CVF International Conference on Computer Vision (ICCV)*, 2019, pp. 2831–2840.
- [17] P. Koniusz, F. Yan, P. Gosselin, and K. Mikołajczyk, "Higher-Order Occurrence Pooling for Bags-of-Words: Visual Concept Detection," *IEEE Transactions on Pattern Analysis and Machine Intelligence*, vol. 39, no. 2, pp. 313–326, 2017.
- [18] P. Koniusz and H. Zhang, "Power normalizations in fine-grained image, few-shot image and graph classification," *IEEE Transactions on Pattern Analysis and Machine Intelligence*, pp. 1–1, 2021.
- [19] P. Li, J. Xie, Q. Wang, and W. Zuo, "Is Second-Order Information Helpful for Large-Scale Visual Recognition?" in *Proceedings of the IEEE International Conference on Computer Vision*, dec 2017, pp. 2089–2097.
- [20] H. Tang, Z. Liu, S. Zhao, Y. Lin, J. Lin, H. Wang, and S. Han, "Searching Efficient 3D Architectures with Sparse Point-Voxel Convolution," in *European Conference on Computer Vision (ECCV)*, 2020.
- [21] P. J. Besl and N. D. McKay, "Method for registration of 3-d shapes," in *Sensor fusion IV: control paradigms and data structures*, vol. 1611. International Society for Optics and Photonics, 1992, pp. 586–606.
- [22] M. Muja and D. G. Lowe, "Fast Approximate Nearest Neighbors with Automatic Algorithm Configuration," *VISAPP (1)*, vol. 2, no. 331–340, p. 2, 2009.
- [23] C. Choy, J. Park, and V. Koltun, "Fully Convolutional Geometric Features," in *Proceedings of the IEEE/CVF International Conference on Computer Vision (ICCV)*, October 2019.
- [24] W. Chen, X. Chen, J. Zhang, and K. Huang, "Beyond triplet loss: a deep quadruplet network for person re-identification," in *Proceedings of the IEEE conference on computer vision and pattern recognition*, 2017, pp. 403–412.
- [25] A. Geiger, P. Lenz, C. Stiller, and R. Urtasun, "Vision meets robotics: The KITTI dataset," *International Journal of Robotics Research*, vol. 32, no. 11, pp. 1231–1237, sep 2013.
- [26] G. Kim, Y. S. Park, Y. Cho, J. Jeong, and A. Kim, "MulRan: Multimodal Range Dataset for Urban Place Recognition," in *2020 IEEE International Conference on Robotics and Automation (ICRA)*, 2020, pp. 6246–6253.